

# Speckle variance optical coherence tomography of the rodent spinal cord: *in vivo* feasibility

David W. Cadotte,<sup>1,2,3,11</sup> Adrian Mariampillai,<sup>4,7,11</sup> Adam Cadotte,<sup>1,3</sup>  
Kenneth K. C. Lee,<sup>4,5</sup> Tim-Rasmus Kiehl,<sup>9</sup> Brian C. Wilson,<sup>6</sup> Michael G. Fehlings,<sup>1,2,3</sup>  
and Victor X. D. Yang<sup>4,5,7,8,10,\*</sup>

<sup>1</sup>Division of Neurosurgery, Toronto Western Hospital, Toronto, Ontario, Canada

<sup>2</sup>Institute of Medical Science, University of Toronto, Toronto, Ontario, Canada

<sup>3</sup>Krembil Neuroscience Centre, Toronto Western Hospital, University Health Network, Toronto, Ontario, Canada

<sup>4</sup>Biophotonics and Bioengineering Laboratory, Ryerson University, Toronto, Ontario, Canada

<sup>5</sup>Department of Electrical and Computer Engineering, University of Toronto, Toronto, Ontario, Canada

<sup>6</sup>Department of Medical Biophysics, University of Toronto, Toronto, ON, Canada

<sup>7</sup>Department of Electrical and Computer Engineering, Ryerson University, Toronto, Ontario, Canada

<sup>8</sup>Department of Medical Imaging, St. Michael's Hospital, Toronto, Ontario, Canada

<sup>9</sup>Department of Pathology, University of Toronto, Toronto, Ontario, Canada

<sup>10</sup>Division of Neurosurgery, St. Michael's Hospital, Toronto, Ontario, Canada

<sup>11</sup>These authors contributed equally to this work.

\*yangv@ee.ryerson.ca

**Abstract:** Optical coherence tomography (OCT) has the combined advantage of high temporal ( $\mu\text{sec}$ ) and spatial ( $<10\mu\text{m}$ ) resolution. These features make it an attractive tool to study the dynamic relationship between neural activity and the surrounding blood vessels in the spinal cord, a topic that is poorly understood. Here we present work that aims to optimize an *in vivo* OCT imaging model of the rodent spinal cord. In this study we image the microvascular networks of both rats and mice using speckle variance OCT. This is the first report of depth resolved imaging of the *in vivo* spinal cord using an entirely endogenous contrast mechanism.

© 2012 Optical Society of America

**OCIS codes:** (110.4500) Optical coherence tomography; (170.3880) Medical and biological imaging; (170.2655) Functional monitoring and imaging.

## References and links

1. J. R. Fetcho and D. M. O'Malley, "Visualization of active neural circuitry in the spinal cord of intact zebrafish," *J. Neurophysiol.* **73**(1), 399–406 (1995).
2. E. I. Solenov, L. Vetrivel, K. Oshio, G. T. Manley, and A. S. Verkman, "Optical measurement of swelling and water transport in spinal cord slices from aquaporin null mice," *J. Neurosci. Methods* **113**(1), 85–90 (2002).
3. S. Sasaki, I. Yazawa, N. Miyakawa, H. Mochida, K. Shinomiya, K. Kamino, Y. Momose-Sato, and K. Sato, "Optical imaging of intrinsic signals induced by peripheral nerve stimulation in the *in vivo* rat spinal cord," *Neuroimage* **17**(3), 1240–1255 (2002).
4. F. Lesage, N. Brieu, S. Dubeau, and E. Beaumont, "Optical imaging of vascular and metabolic responses in the lumbar spinal cord after T10 transection in rats," *Neurosci. Lett.* **454**(1), 105–109 (2009).
5. D. Huang, E. A. Swanson, C. P. Lin, J. S. Schuman, W. G. Stinson, W. Chang, M. R. Hee, T. Flotte, K. Gregory, C. A. Puliafito, and J. G. Fujimoto, "Optical coherence tomography," *Science* **254**(5035), 1178–1181 (1991).
6. V. J. Srinivasan, S. Sakadžić, I. Gorczynska, S. Ruvinskaya, W. Wu, J. G. Fujimoto, and D. A. Boas, "Depth-resolved microscopy of cortical hemodynamics with optical coherence tomography," *Opt. Lett.* **34**(20), 3086–3088 (2009).
7. V. J. Srinivasan, S. Sakadžić, I. Gorczynska, S. Ruvinskaya, W. Wu, J. G. Fujimoto, and D. A. Boas, "Quantitative cerebral blood flow with optical coherence tomography," *Opt. Express* **18**(3), 2477–2494 (2010).
8. V. J. Srinivasan, D. N. Atochin, H. Radhakrishnan, J. Y. Jiang, S. Ruvinskaya, W. Wu, S. Barry, A. E. Cable, C. Ayata, P. L. Huang, and D. A. Boas, "Optical coherence tomography for the quantitative study of cerebrovascular physiology," *J. Cereb. Blood Flow Metab.* **31**(6), 1339–1345 (2011).
9. Y. Jia, P. Li, S. Dziennis, and R. K. Wang, "Responses of peripheral blood flow to acute hypoxia and hyperoxia as measured by optical microangiography," *PLoS ONE* **6**(10), e26802 (2011).
10. B. T. Cox and P. C. Beard, "Photoacoustic tomography with a single detector in a reverberant cavity," *J. Acoust. Soc. Am.* **125**(3), 1426–1436 (2009).

11. D. Razansky, N. C. Deliolanis, C. Vinegoni, and V. Ntziachristos, "Deep tissue optical and optoacoustic molecular imaging technologies for pre-clinical research and drug discovery," *Curr. Pharm. Biotechnol.* **13**(4), 504–522 (2012).
12. J. Laufer, B. Cox, E. Zhang, and P. Beard, "Quantitative determination of chromophore concentrations from 2D photoacoustic images using a nonlinear model-based inversion scheme," *Appl. Opt.* **49**(8), 1219–1233 (2010).
13. S. Ye, R. Yang, J. Xiong, K. K. Shung, Q. Zhou, C. Li, and Q. Ren, "Label-free imaging of zebrafish larvae *in vivo* by photoacoustic microscopy," *Biomed. Opt. Express* **3**(2), 360–365 (2012).
14. R. C. Mesquita, T. Durduran, G. Yu, E. M. Buckley, M. N. Kim, C. Zhou, R. Choe, U. Sunar, and A. G. Yodh, "Direct measurement of tissue blood flow and metabolism with diffuse optics," *Philos. Transact. A Math. Phys. Eng. Sci.* **369**(1955), 4390–4406 (2011).
15. G. Liu, W. Qi, L. Yu, and Z. Chen, "Real-time bulk-motion-correction free Doppler variance optical coherence tomography for choroidal capillary vasculature imaging," *Opt. Express* **19**(4), 3657–3666 (2011).
16. A. Mariampillai, B. A. Standish, E. H. Moriyama, M. Khurana, N. R. Munce, M. K. Leung, J. Jiang, A. Cable, B. C. Wilson, I. A. Vitkin, and V. X. Yang, "Speckle variance detection of microvasculature using swept-source optical coherence tomography," *Opt. Lett.* **33**(13), 1530–1532 (2008).
17. A. Mariampillai, M. K. Leung, M. Jarvi, B. A. Standish, K. Lee, B. C. Wilson, A. Vitkin, and V. X. Yang, "Optimized speckle variance OCT imaging of microvasculature," *Opt. Lett.* **35**(8), 1257–1259 (2010).
18. V. J. Srinivasan, J. Y. Jiang, M. A. Yaseen, H. Radhakrishnan, W. Wu, S. Barry, A. E. Cable, and D. A. Boas, "Rapid volumetric angiography of cortical microvasculature with optical coherence tomography," *Opt. Lett.* **35**(1), 43–45 (2010).
19. W.-Y. Oh, B. J. Vakoc, M. Shishkov, G. J. Tearney, and B. E. Bouma, ">400 kHz repetition rate wavelength-swept laser and application to high-speed optical frequency domain imaging," *Opt. Lett.* **35**(17), 2919–2921 (2010).
20. K. Zhang and J. U. Kang, "Real-time 4D signal processing and visualization using graphics processing unit on a regular nonlinear-k Fourier-domain OCT system," *Opt. Express* **18**(11), 11772–11784 (2010).
21. M. R. Chatni, J. Yao, A. Danielli, C. P. Favazza, K. I. Maslov, and L. V. Wang, "Functional photoacoustic microscopy of pH," *J. Biomed. Opt.* **16**(10), 100503 (2011).
22. F. E. Robles, C. Wilson, G. Grant, and A. Wax, "Molecular imaging true-colour spectroscopic optical coherence tomography," *Nat. Photonics* **5**(12), 744–747 (2011).
23. J. K. Leitch, C. R. Figley, and P. W. Stroman, "Applying functional MRI to the spinal cord and brainstem," *Magn. Reson. Imaging* **28**(8), 1225–1233 (2010).
24. P. Enager, H. Piilgaard, N. Offenhauser, A. Kocharyan, P. Fernandes, E. Hamel, and M. Lauritzen, "Pathway-specific variations in neurovascular and neurometabolic coupling in rat primary somatosensory cortex," *J. Cereb. Blood Flow Metab.* **29**(5), 976–986 (2009).
25. D. Attwell, A. M. Buchan, S. Charpak, M. Lauritzen, B. A. Macvicar, and E. A. Newman, "Glial and neuronal control of brain blood flow," *Nature* **468**(7321), 232–243 (2010).

## 1. Introduction

Optical imaging of the spinal cord has made considerable advancements since the first published reports in mid-1990's. These early experiments used calcium dyes that fluoresced with neural activity; the combination of the transparent larval zebrafish with confocal microscopy allowed for the *in vivo* study of motor circuits of the spinal cord [1]. While revolutionary for its ability to visualize the activity of neuronal populations interacting with each other, confocal microscopy is limited by its penetration depth and the use of exogenous voltage sensitive dyes. Other optical imaging methods utilized in the spinal cord include light transmittance assays in thin *ex vivo* spinal cord slices [2] and the use of optical reflectance signals from the dorsal surface of an *in vivo* rodent model [3]. More recently, laser speckle imaging was used in the setting of a rodent spinal cord injury model whereby the light reflectance was used to estimate the spinal cord vascular response to electrical stimulation before and after traumatic spinal cord injury [4]. The drawback of each of these techniques is the lack of depth resolution into the spinal cord beyond approximately 300  $\mu\text{m}$ .

Optical coherence tomography (OCT), based on low coherence interferometry, offers the unique advantage of high spatial and temporal resolution [5]. This technique has been recently applied to perform depth-resolved measurements of blood vessel diameter, blood flow and total hemoglobin in the rat brain [6]. In this and other works, Boas' group move beyond surface scatter changes reported by others and demonstrate methods for three-dimensional imaging of the rat cortex and provide measurements of two dimensional blood flow that correspond with autoradiographic techniques [6–8]. Several other important methods have recently been put forward, each aiming to maximize both temporal and spatial resolution at

the tissue depth required for the intended application. Optical microangiography (OMAG) uses intrinsic optical scattering signals backscattered from tissue to gauge microvascular caliber, microvascular density and the changes that occur to vessels in response to physiological challenges such as hypoxia or hyperoxia [9]. Optical frequency domain imaging (OFDI) is another technique that has emerged to investigate aspects of tissue biology requiring high spatial and temporal resolution without altering the natural state of the tissue. The combination of optical contrast with ultrasonic detection has also been successfully adopted in the form of both photoacoustic computed tomography (PACT) and photoacoustic microscopy (PAM) [10–12]. These techniques use an exciting laser on tissue samples to generate thermal expansion that can be subsequently detected as an ultrasound wave. PAM was most recently used to obtain high-resolution images of living zebrafish larva [13], an application that could be easily expanded to other animal models. Our understanding of tumor angiogenesis and morphological characteristics of growing microvascular networks has benefited [10]. Diffuse correlation spectroscopy (DCS) has recently progressed from bench to bedside where quantitative measurements of blood flow in the human brain have been compared with multiple existing techniques including arterial spin labeled MRI, xenon-CT and Doppler ultrasound [14]. Moving beyond the characteristics of changes in flow and morphology, the combination of hyperspectral imaging with spectral domain OCT provide information on the shear rate on vessel walls during tumor growth [12]. A deeper understanding of the biophysical forces involved with changing vessels could certainly prove valuable beyond a richer understanding of antiangiogenesis therapies, and would be particularly useful in understanding the pathobiology of vascular malformation diseases such as arteriovenous malformations or hereditary aneurysm syndromes. Another important aspect of imaging biological tissues is the consideration of motion. An elegant report by Chen's group [15] describes the use of Doppler-variance OCT whereby they perform retinal vascular imaging that is largely insensitive to bulk motion, a clear advantage for future applications to ophthalmology centered diagnosis and patient management.

Speckle-variance OCT (SV-OCT) has the capability of depth resolved three-dimensional imaging over a period of time, usually measured in seconds. The speckle pattern relies on the spatial coherence properties of the optical signal back reflected from the tissue being sampled. This endogenous contrast mechanism relies on the mathematical analysis of the dynamic speckle pattern generated by the motion of erythrocytes in the artery, vein or capillary bed. Recently, Mariampillai *et al.* introduced microvascular imaging based on inter-frame speckle variance in a swept-source OCT system [16,17]. This method calculates the inter-frame intensity variance of a sequence of structural images. The main advantage is its depth resolution and insensitivity to Doppler angle-dependent contrast allowing for three-dimensional imaging of microvascular networks at greater tissue depths. The obvious downside of the method is its sensitivity to bulk motion.

Here, we provide the first report of depth resolved OCT of the spinal cord using an entirely endogenous contrast mechanism taking advantage of the speckle variance approach recently described by Mariampillai [16,17]. We demonstrate methods to optimize bulk motion correction and image a 3D volume of both the rat and mouse spinal cord.

## 2. Materials and methods

All animal protocols were approved by the animal care committee at the University Health Network, Toronto Western Hospital and Princess Margaret Hospital.

*Rat spinal cord preparation:* Male Wistar rats weighing approximately 150g were induced with 2.5% isoflurane inhalational anesthesia. A rectal temperature probe was inserted and body temperature was maintained at  $37^{\circ}\text{C} \pm 0.5^{\circ}\text{C}$  using a heated gel pack. A dorsal tail vein catheter was inserted for intravenous access. Maintenance fluids were given at a rate of 2mL/kg/hr. A dorsal laminectomy was performed at the L1 to L2 level according to previous published methods [16]. Following the laminectomy, a tracheostomy was performed and

mechanical ventilation (2% isoflurane at 2 mL tidal volume and 55 breaths per minute) was initiated using a Harvard Rodent Ventilator. The animal was then paralyzed using an infusion of pancuronium bromide (2 mg/kg/hr). This was performed so as to conduct breath-hold periods during the imaging protocol so as to stabilize the spine. The spine was then mechanically fixed by performing an extra-cavitary dissection around the transverse process of the T12 vertebral body and fixing halo pins (DePuy) into the anterior vertebral body and fixed to a standard imaging breadboard using a homemade jig (Figs. 2A and 2B below). The imaging protocol, as described below, was initiated

*Mouse spinal cord preparation:* C57BL/6 mice weighing approximately 35g were anesthetized with a mixture of xylazine (10 mg/kg) and ketamine (70 mg/kg) intraperitoneal (i.p.). The mouse spinal cord was prepared in a similar fashion to that of the rat with the following exceptions: Cardio-respiratory motion was found to be less in the lumbar spine of a mouse than a rat, therefore we did not utilize a breath-hold paradigm; the animal was maintained on i.p. anesthesia and a tracheostomy was not performed; the mouse spinal column was held in position using a homemade jig as outlined in Fig. 3A below. Briefly, we used two pairs of forceps to stabilize the spinal column above and below the exposed spinal cord. These forceps were gently held in position using a fastening device so as to put gentle pressure on the vertebral bodies without damaging the bony spine. These forceps were then fixed to the imaging breadboard.

*Histology:* Spinal cord specimens were removed from the examined animals after completion of the imaging protocol and placed in formalin. Standard H&E stains were performed to compare histological anatomy with OCT derived anatomical information.

*Imaging System:* A schematic of the swept source OCT system is illustrated in Fig. 1. The laser, data acquisition and software were specifically designed to enable continuous real-time processing and display of both structural and speckle variance data while simultaneously saving recalibrated fringe data at an A-scan rate of 108 kHz. Briefly, speckle variance OCT is an inter-frame vascular detection technique that unlike phase sensitive processing is not affected by Doppler angle or the flow velocity. The technique is similar to power Doppler and OMAG techniques in that it measures residual signal power after filtering out static tissue components. The algorithm performs a straightforward variance calculation on the non-log compressed intensity data at each pixel location within a set of N frames (referred to as the gate length). The resulting set of variance images can either be thresholded manually or by using the structural data, which is typically more effective in the presence of residual motion [18]. The swept source laser design is a buffered polygon ring cavity laser where a 600 lines/mm diffraction grating (GR25-0613, Thorlabs) was chosen to create the necessary dead time between laser sweeps to enable buffering from 54 kHz to 108 kHz [19]. Standard techniques for triggering and recalibration were used in this system [16]. The analog signals were fed in to a data acquisition system and digitized at 250 MS/s (ATS9350, AlazarTech), which was transferred to the memory on a video graphics card (GeForce GTX 460 1GB, NVIDIA). Custom-written kernels together with built-in CUDA libraries (i.e. cudpp, cufft) were used to manipulate and reconstruct structural and speckle variance OCT images on the multiple cores (336) of the GPU, which enables massive parallel data processing and not only dramatically enhance the data throughput when compared to processing using only the CPU but also concurrently free up CPU resources [20]. Another advantage for processing data directly on the graphics card is that the reconstructed OCT images can be displayed without any additional memory transactions. The above setup allows real-time acquisition, processing, and display only limited by the A-scan rate of the laser. Finally, the recalibrated fringe data was saved to a PCIe solid state drive (RevoDrive3 X2 series, OCZ) for post processing and 3D visualization.

*Imaging protocol:* The anesthetized animal was placed under the scan head of the imaging system and properly positioned using the real-time 2D-display for feedback. For both 2D and 3D imaging we chose to use 512 A-scans per image over a scan distance of 3mm, this resulted

in an image acquisition rate of greater than 200 fps. We found that this imaging speed was sufficient to eliminate most of the effects of residual bulk tissue motion. Average structural and speckle variance images were calculated using a gate length of  $N = 4$  and displayed in real-time at 50 fps. For 3D imaging we acquired 3000 B-mode images over a  $3\text{mm}(x) \times 3\text{mm}(y) \times 2\text{mm}(z)$  volume in approximately 15 seconds for post processing. The large amount of oversampling done in the  $y$ -direction minimized the amount of static structure decorrelation when calculating the speckle variance image.

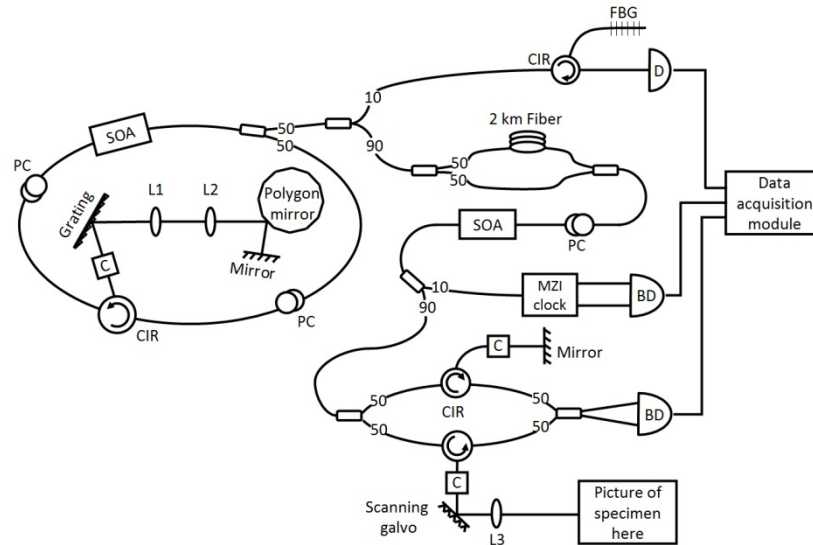


Fig. 1. Schematic diagram of the swept-source OCT system used in this set of experiments. A 54 kHz polygon filter based swept source laser was used with grating that enables buffering to 108kHz and post amplified by a semiconductor optical amplifier (SOA). The coherence of the laser source is approximately 1.5 mm. PC: polarization controller; CIR: optical circulator; C: collimator; L: lenses; FBG: fiber Bragg gratings; D: photodetector; BD: balanced detector.

**3D Speckle variance post processing:** For 3D visualization of vascular structures done in post processing we continued to use a gate length of  $N = 4$ . Next, an user defined threshold based on the structural images was applied to the image stack before the application of median ( $3 \times 3$ ) and Gaussian ( $3 \times 3, \sigma = 0.5$ ) filters to each of the  $x$ - $z$  images in the stack. Lastly, the 3D stack was projected in the  $z$ -direction to provide an *en face* 2D image of the vascular structures.

### 3. Results

Figure 2 demonstrates the results for a rat spinal cord model. In the absence of spinal stabilization, we observed bulk cardio-respiratory motion of the rat spinal column on the order of millimeters in both the rostral-caudal and anterior-posterior direction (not shown). Performing an extra-cavitary lateral dissection around the transverse process one vertebral body above the level of the exposed spinal cord allowed for the placement of motion-stabilization pin into the anterior vertebral body that was also fixed to the imaging breadboard. This minimized cord motion to approximately  $40\mu\text{m}$  in the anterior-posterior direction, quantified with the OCT apparatus (Fig. 2, panel C). By employing a brief breath-hold ( $<15$  sec), we were able to further reduce bulk motion to  $<8\mu\text{m}$  (Fig. 2, panel C). During the breath-hold cycle, we acquired structural OCT data (panel E). Observed are the overlying dura matter, the underlying cerebrospinal fluid, the dorsal vein and the spinal cord. The rather large dorsal venous, consisting of the median dorsal vein and tributaries (best observed on the SV-OCT image, panel F) limit depth resolved images to approximately  $200\mu\text{m}$ . A histology

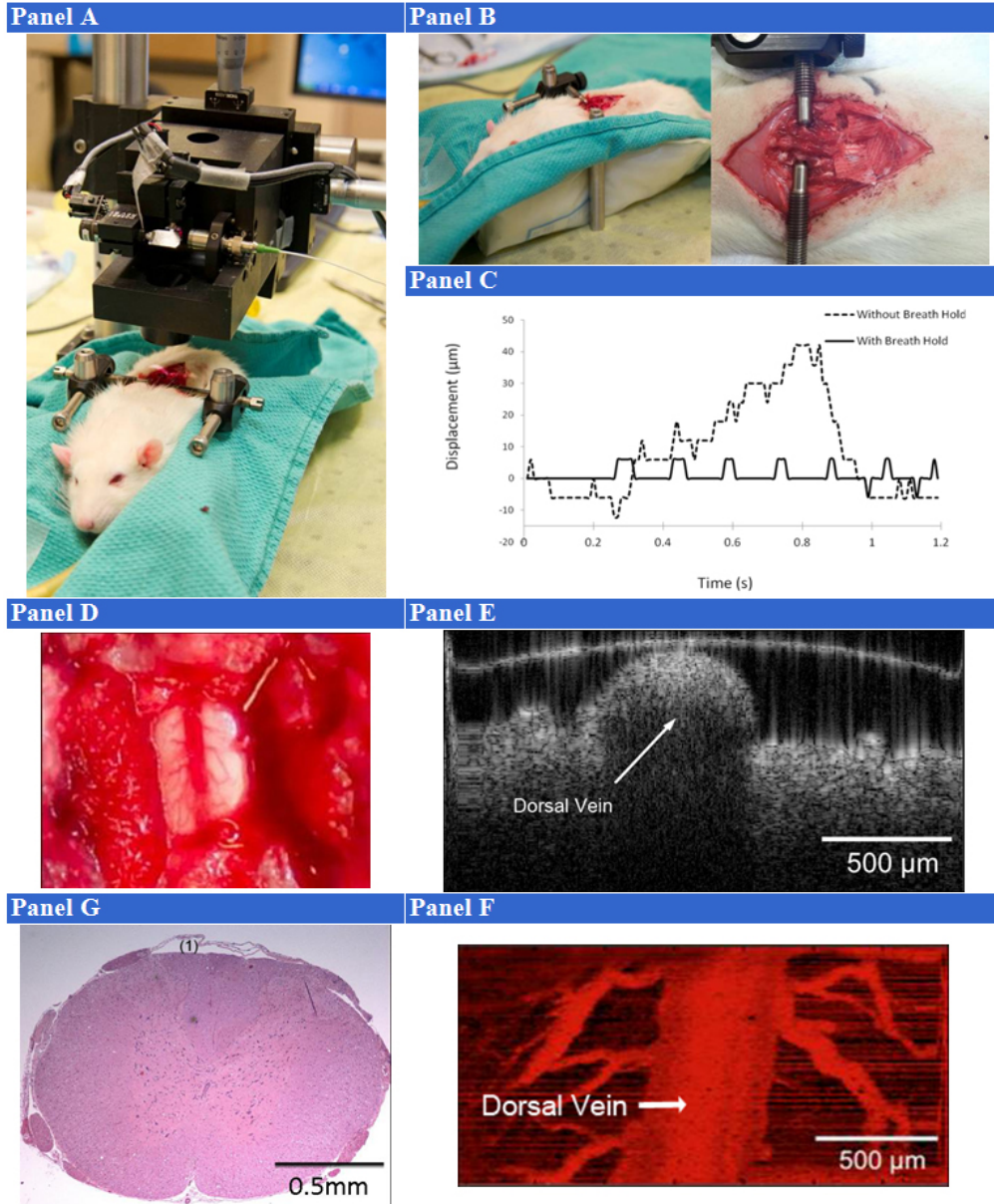


Fig. 2. Experimental setup of rat SV-OCT. Panel A shows an overview of the imaging station with the male Wistar rat pinned to the imaging breadboard. Panel B shows a close up of the pin fixation. The animal is resting on a heated gel pack to maintain 37°C body temperature (panel B). The animal underwent tracheotomy and is receiving inhalational anesthetic. Breath-hold was conducted to reduce bulk motion from >40µm in the anterior-posterior direction to <8µm (panel C). A close up of the exposed spinal cord is shown in panel D. Panel E demonstrates structural OCT data. Panel F shows an en face projection of the SV-OCT data. A histology specimen is provided in panel G for comparison, with the dorsal vein (1) marked.

specimen is provided in panel G that shows the collapsed dorsal vein and the spinal cord gray matter and white matter.

Figure 3 demonstrates results for the mouse spinal cord. We found that the cardio-respiratory motion in the lumbar region of the mouse spinal cord was significantly less than that of the rat (not shown). With a rather simple spinal stabilization jig (Fig. 3, panel A), we



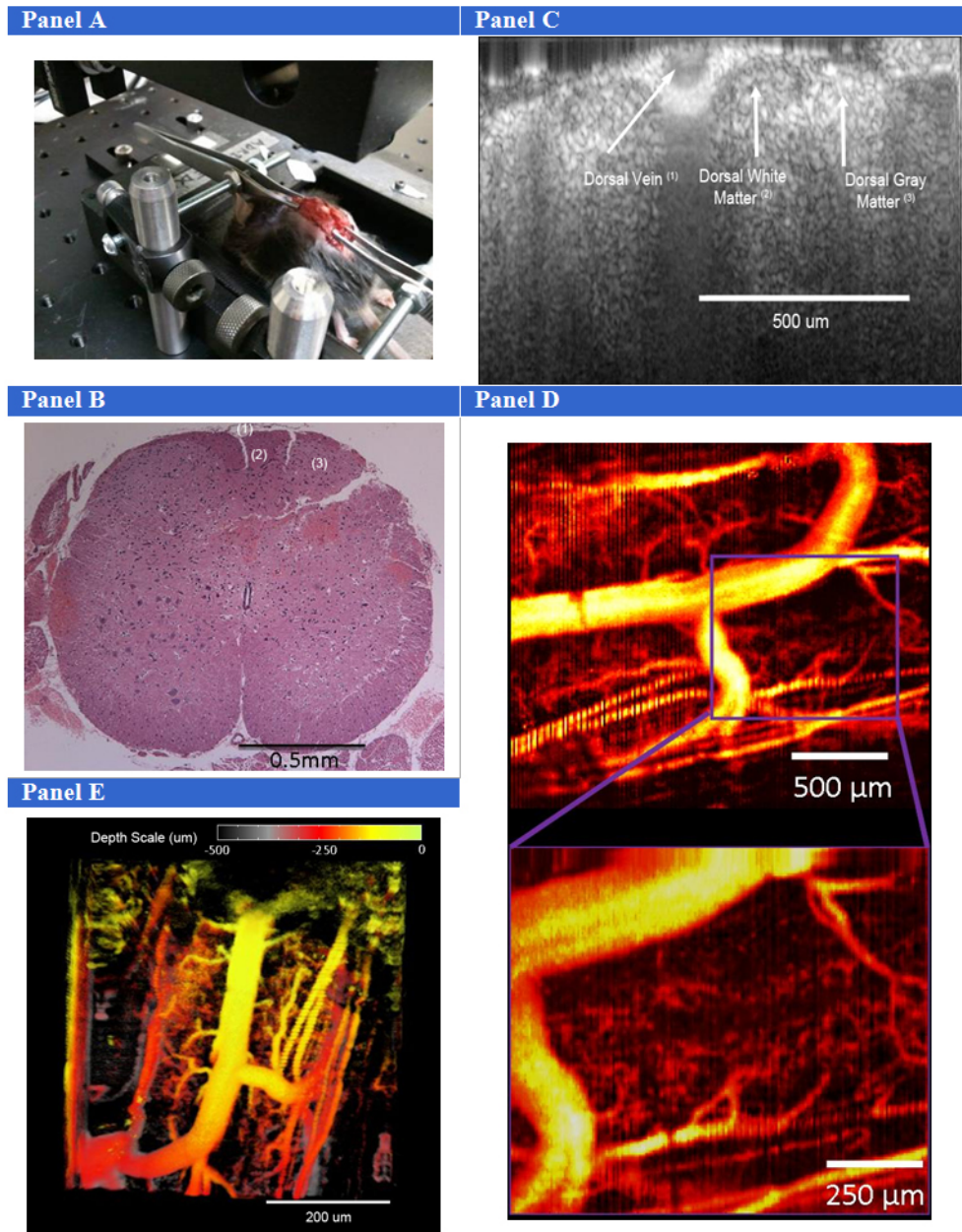


Fig. 3. Experimental setup of mouse SV-OCT imaging. Bulk motion correction of the spinal column was carried out with a homemade jig as shown in panel A. Briefly, we used two pairs of forceps to gently grasp the spinal column one vertebral body level above and below the exposed spinal cord. A histology specimen is provided in panel B that demonstrates the dorsal vein (1), dorsal white matter (2) and dorsal gray matter (3). A structural OCT image is shown in panel C that demonstrates the dorsal vein, dorsal white and gray matter. SV-OCT images are shown in panel D demonstrating the microvascular network of the mouse spinal cord resolving vessels with a diameter of approximately 10-20 $\mu$ m. Panel E illustrates a depth dependent false color map of the mouse spinal cord.

were able to reduce bulk motion of the spinal cord in order to acquire SV-OCT data. We demonstrate contrast between the dorsal gray and white matter in structural OCT data (Fig. 3, compare histology in panel B with structural OCT image in panel C) to a depth of approximately 500 $\mu\text{m}$ . SV-OCT is shown in panel D along with a depth dependent false color map in panel E. A magnified image on the right demonstrates vessels on the order of 10-20 $\mu\text{m}$ . A three-dimensional structural OCT volume (3mm(x)  $\times$  3mm (y)  $\times$  2mm (z)) can be viewed in Fig. 4 and a three-dimensional SV-OCT volume can be viewed in Fig. 5.

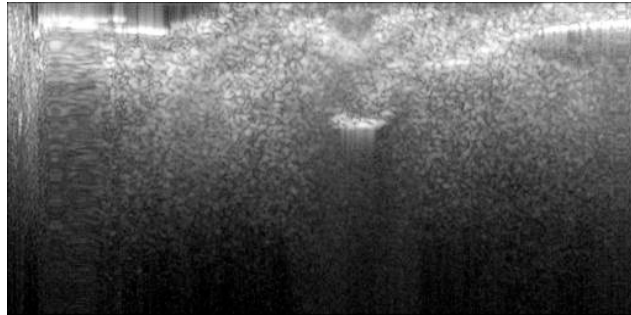


Fig. 4. A three-dimensional structural OCT volume (3mm(x)  $\times$  3mm (y)  $\times$  2mm (z)) of the mouse spinal cord ([Media 1](#)).

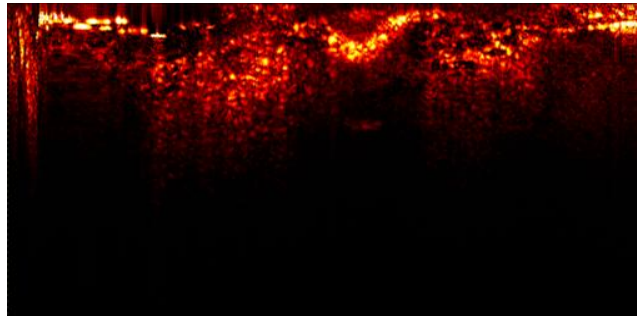


Fig. 5. A three-dimensional SV-OCT volume (3mm(x)  $\times$  3mm (y)  $\times$  2mm (z)) of the mouse spinal cord ([Media 2](#)).

#### 4. Discussion

Here we demonstrate the use of SV-OCT to image microvascular networks of the rat and mouse spinal cord. While speckle variance imaging offers the combined advantage depth resolved imaging of microvascular networks without the limitation of sensitivity to the Doppler angle, bulk motion can limit the use of this technique. We present two different techniques to limit bulk motion in the rat and mouse spinal cord. We acquired vascular imaging to a depth of approximately 200 $\mu\text{m}$  in the rat spinal cord. The large dorsal vein and extensive tributaries prevented imaging microvascular networks beyond 200 $\mu\text{m}$ . Thus, experiments designed to investigate the most superficial aspects of the dorsal horn, limited to Rexed laminae I and II are feasible.

The mouse spinal cord exhibited both less cardio-respiratory motion and a less extensive network of dorsal venous tributaries. We were thus able to image approximately 500 $\mu\text{m}$  into the mouse spinal cord, visualizing the entire dorsal gray matter and a portion of the ventral gray matter. The gray matter of the spinal cord contains neuronal cell bodies, synapses and interneurons. The surrounding white matter is composed of myelinated axons responsible for transmitting neuronal signals to and from the brain. Given the bulk motion correction and depth resolved imaging in the mouse spinal cord, it will be possible to investigate



microvascular changes in the dorsal horn of the spinal cord in response to somatosensory stimulation.

Over the past few years speckle variance and related OCT methods for high sensitive vascular detection have been applied to a number of preclinical and clinical methods. However, OCT is not the only imaging modality for assessment of superficial vascular networks. Recently, Photo-Acoustic Microscopy (PAM) has also been used very successfully to image superficial vascular networks [21]. With PAM vascular networks can be assessed with a transverse resolution of 50  $\mu\text{m}$  to a depth of approximately 3mm (assuming a 50Mhz transducer). For certain applications this increase in depth of penetration (vs. 1.0-1.5 mm with OCT) can be very advantageous even though there is a significant decrease in transverse resolution. Perhaps one of the most important benefits of PAM is the ability to readily measure de-oxy and oxy hemoglobin levels and thus distinguish the venous and arterial systems. Recent advances in spectroscopic OCT may convey the same benefit to OCT, but to date these techniques have not become very prevalent [22]. Two drawbacks of PAM are the relatively long acquisition times and the need of a coupling medium between the transducer and tissue surface. Both of these drawbacks arise because signals are received acoustically and are thus limited by the propagation speed of sound, these issues may limit the use of PAM for intra-operative applications.

## 5. Conclusion

Here we demonstrate the application of SV-OCT to image the rodent spinal cord. We address the limitation of speckle variance imaging and provide two different techniques to correct for bulk motion in the spinal cord. We provide the first report of imaging the three-dimensional microvascular network of the spinal cord using an entirely endogenous contrast mechanism. In addition, we provide an estimation of the depth resolution possible based on Rexed laminae such that specific neuroscience questions can be framed around the current limitations of optical coherence tomography.

The relationship between neural activity and blood flow, referred to as neurovascular coupling, has almost exclusively been studied within the brain. The neuroscience community has benefited enormously from understanding this relationship, as it is the foundation for functional MRI studies whose signal is generated based on local increases in blood flow in response to neuronal activity, a phenomenon referred to as functional hyperemia. Functional MRI studies of the human spinal cord are emerging in increasing numbers due to recent technological advancements in managing magnetic susceptibility artifacts intrinsic to the spinal column and cardio-respiratory motion [23]. It is currently not known if the neurovascular signaling mechanisms underlying functional hyperemia in the spinal cord are similar to those in the cerebral cortex. As recently established, neurovascular coupling mechanisms differ across neuroanatomical pathways in the cerebral cortex and across brain regions [24,25]. Whether or not these mechanistic differences exist in the evolutionary older spinal cord remains to be determined as do their effect on functional hyperemia. Optical techniques will surely play a role in uncovering this mystery both in the healthy spinal cord and in certain disease states, including traumatic spinal cord injury.

## Acknowledgments

The authors acknowledge funding support from the Krembil Neuroscience Center at Toronto Western Hospital, University Health Network. In addition, we received funding support from NSERC, ERA, CIHR and Ryerson University.